



# Geophysical modeling applied to hydrogeology of fractured crystalline terrain, Juá District, CE.

Marcos César Soares de Queiroz<sup>\*1</sup>, Mônica G. Von Huelsen<sup>2</sup>, <sup>1</sup>CPRM, <sup>2</sup>UNB

Copyright 2023, SBGf - Sociedade Brasileira de Geofísica

This paper was prepared for presentation during the 18<sup>th</sup> International Congress of the Brazilian Geophysical Society held in Rio de Janeiro, Brazil, 16-19 October 2023.

Contents of this paper were reviewed by the Technical Committee of the 18<sup>th</sup> International Congress of the Brazilian Geophysical Society and do not necessarily represent any position of the SBGf, its officers or members. Electronic reproduction or storage of any part of this paper for commercial purposes without the written consent of the Brazilian Geophysical Society is prohibited.

## Abstract

A portion of the northeast region of Brazil is strongly influenced by the semi-arid climate, which is defined by periodic droughts, and compromises the water supply through surface reservoirs. The subsurface of these areas has a crystalline basement and the accumulation of groundwater is controlled by networks of fractures. To mitigate the problems in these environments, airborne geophysical methods: FDEM (Frequency Domain Electromagnetic Method) and magnetometry are included as potential non-invasive tools to map the distribution of groundwater resources. This work presents a geophysical model that describes the behavior of conductive and anomalous magnetic sources at depth. The integration of these models with geological data contributes significantly to the efficiency in the location of groundwater wells.

## Introduction

The study region is in the drought polygon, and water scarcity is one of the most recurrent problems in these areas. In addition, the role of public institutions is limited, and the geographical distribution of small villages is unfavorable, as they are separated from each other by kilometers. Another limiting factor for water supply is the socioeconomic dynamics. Groundwater reserves are usually the only source of livelihood for this population, and the location of groundwater wells is a viable alternative.

The Brazilian northeast is constituted by a crystalline basement of granitic and migmatitic composition, which indicates low intergranular porosity, disfavoring or eliminating the water storage capacity in its interstices. When these rocks are subjected to stresses and strains that can be caused by tectonic movements of crustal accommodation and other geological factors, fracture zones develop that have the capacity to store groundwater from precipitation (Marques, 1995; Coriolano 2002; Nascimento da Silva, 2004; Souza Filho *et al.*, 2010).

In this perspective, the Project Groundwater in the Northeast of Brazil (PROASNE), led by the Geological Service of Brazil (CPRM) and by the Geological Survey of Canada (GSC), and executed by Lasa Engenharia Prospecções S/A in three locations: Juá-CE, Samambaia-RN, and Serrinha-PE, had its efforts directed to the

development and application of sustainable solutions to the supply of areas affected by drought.

This international collaborative project conducted airborne geophysical surveys, which included controlled-source electromagnetic field measurements in the frequency domain and natural magnetic field measurements, and provided a good overview for the state-of-the-art of fractured crystalline terrains due to the high resolution obtained in the acquired data.

Applications of airborne electromagnetic measurements for hydrogeophysics can be found in the literatures such as groundwater mapping and salinity distribution (Sattel & Kgotlhang, 2004; e.g., Bedrosian *et al.*, 2016; Chongo *et al.*, 2015; Siemon *et al.*, 2015; King *et al.*, 2018), and groundwater discharge in coastal areas (Paepen *et al.*, 2020).

FDEM data inversion and Conductivity Depth Imaging (CDI) combined with Euler solutions for the magnetic data define the methodology outlined in this work. Obtaining a conductivity model and identifying geologically consistent magnetic sources can be a potential tool for mapping water resources. For the application of this methodology, the Juá district, located in the municipality of Irauçuba, state of Ceará, was chosen as the study area (figure 1).

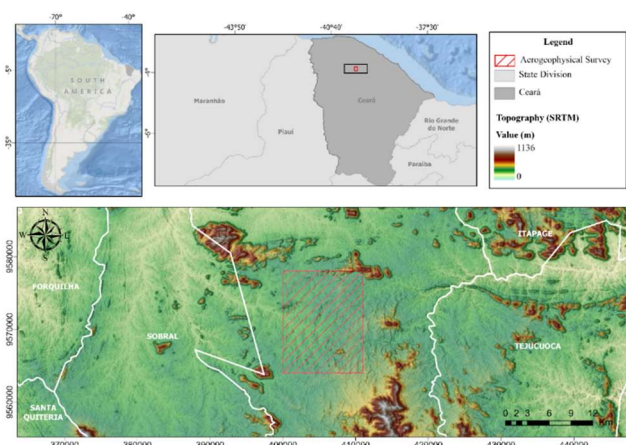


Figure 1- Location and topography map of the study area, Juá-CE.

## Geological Setting

The Juá District is located in the Borborema Province (Almeida *et al.*, 1977), which has several active faults and is divided by a complex system of shear zones that limit different lithospheric domains (Bezerra *et al.*, 2011). The area consists mainly of crystalline rocks of the Precambrian period formed and reworked in the brasiliano cycle and overlain by alluvial deposits.

Precambrian rocks are represented by Paleoproterozoic high grade metamorphic rocks; supracrustal rock sequences and intrusive rocks (Neoproterozoic). The Cenozoic is represented by sparse residual sedimentary covers and alluvial deposits (Santos de Menezes, 2017).

Three Precambrian units are recognized in the study area: i) Four supracrustal sequences to the south and northwest referring to the Ceará complex of Mesoproterozoic age (Arthaud et al., 1998); ii) Orthogneisses and migmatites to the north and west; iii) Granitoids of batholithic dimension to the northeast. Figure 2 characterizes the geological map of the airborne geophysical survey area.

Studies on seismic activity have been carried out in Irauçuba since 1991. In the southwestern region of the study area is the record of an event that may be related to a seismogenic fault reported in Santos de Menezes (2017). This event was plotted to the result obtained by inversion of the electromagnetic data in order to observe the conductive behavior.

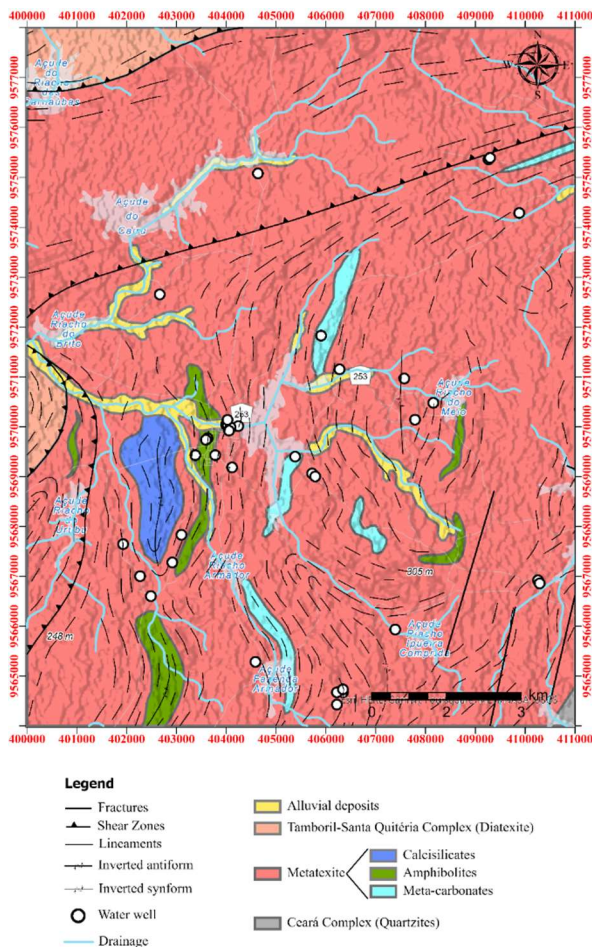


**Figure 2-** Geological map of the airborne geophysical survey area.

## Method

The Electromagnetic induction method

The active electromagnetic methods are based on the contrast of the electromagnetic properties of the soil. The feasibility of using this method to study an anomalous body depends on the contrast of properties of the environment around it, the nature of the materials, the depth, the way they are arranged, and their proximity to the water table. If these contrasts are large enough, then the anomalies will be detected.

The methodology applied in this work is based on the basic theory of the electromagnetic method in the frequency domain. The theoretical basis consists of circulating an alternating electric current, which has a constant frequency, in a transmitting coil ( $T_x$ ), resulting in a primary electromagnetic field ( $H_p$ ). The propagation of this field underground, where the conductive medium induces secondary electrical currents that produce a secondary electromagnetic field ( $H_s$ ) proportional to the induced current.

A part of the secondary field induces electric currents in a receiving coil ( $R_x$ ), positioned within the area of influence of the primary and secondary fields. The potential difference (d.d.p.) associated with the electrical current induced in the receiving coil is directly proportional to the electrical conductivity of the terrain. Assume that the ratio of the distance of the coils ( $T_x$ ) and ( $R_x$ ) to the skin depth is known as the induction number ( $B$ ), and that if the induction number is low ( $B \ll 1$ ), then the ratio of the secondary magnetic field ( $H_s$ ) to the primary in the coil ( $R_x$ ) obeys a linear relationship in the coil ( $R_x$ ) directly proportional to the apparent conductivity (Mc Neill, 1991).

$$\sigma_a = \left( \frac{4 \left( \frac{H_s}{H_p} \right)^2}{\mu_0 \omega s^2} \right)$$

where ( $f$ ) = frequency of the electric current flowing in the coil ( $T_x$ ), in (Hz); ( $\omega$ ) = angular frequency, in ( $rad/s$ ); ( $\mu_0$ ) = magnetic permeability of the vacuum, in ( $H/m$ ); ( $s$ ) = spacing between coils ( $T_x$ ) and ( $R_x$ ), in meters. This relation allows the construction of instruments that make a direct reading of the electrical conductivity (Siemens/m) at a predetermined depth. The apparent conductivity was calculated based on the phase and quadrature components of the secondary magnetic field and in the pseudo-layer model defined by (Fraser, 1978). This model consists of a resistive layer over a conductive semi-space, and images of the conductivity were obtained for three frequencies and two geometries (coaxial and coplanar). In this work, the images of conductivity in coplanar geometry will be analyzed as they present better resolution.

## FDEM data Inversion

The algorithm used for inversion assumes a set of contiguous rectangular prisms. Each prism has a physical property contrast value (Ellis et al., 2012; Richarte et al.,

2018). The inversion model follows the solution of the direct modeling equation:

$$E \cdot m = d$$

where ( $m$ ) is the vector of the model that contains the values of the physical properties of the cells; ( $d$ ) is the data in the matrix-vector and ( $E$ ) is the sensitivity matrix that quantifies the contribution of cells in relation to the observed data value (Ellis et al., 2012; Richarte et al., 2018). The vector ( $m$ ) represents the conductivity ( $\sigma$ ) and the vector ( $d$ ) the electromagnetic data. The resulting voxel (three-dimensional model) is based on a Cartesian system, where X is east, Y is north, and Z points vertically down. The inverse solution was obtained using Tikhonov regularization minimizing a total objective function with bounded constraints (Richarte et al., 2018):

$$\min(\phi) = \phi d + \mu \phi m$$

$$m_{min} \leq m \leq m_{max}$$

where ( $m$ ) is the regularization parameter; ( $\phi d$ ) the data misfit and ( $\phi m$ ) is the misfit function. The parameters ( $m_{min}$ ) and ( $m_{max}$ ) are the lower and upper limits of the distribution of physical properties (Richarte et al., 2018). This step helps control the distribution of the conductivity contrast response that results in the inverse model.

### Conductivity-depth imaging

The CDI is a section of conductivity by the depth that represents here an interpretation of airborne EM data. The purpose of imaging is to transform the responses obtained through the airborne electromagnetic (AEM) method to an image of conductivity by depth (CDI) and thus extract information from the target's geometry and conductivity to facilitate geological interpretation (Huelsen., 2007). The sampled relationship of apparent conductivity to depth is given by:

$$\delta = \left(\frac{2}{\omega \mu \sigma}\right)^{1/2} = k \left(\frac{1}{f \sigma}\right)^{1/2}$$

Where delta ( $\delta$ ) is the depth of penetration, given by the relationship between frequency and conductivity of the medium and a ( $k$ ) factor, this equation is called the skin depth equation.

The location coordinates of the anomalous magnetic sources were identified by Euler deconvolution of structural index 1 and tolerance 10%. The solutions showed vertical and subvertical magnetic contacts in the models obtained by the CDI's.

### Acquisition and Processing

The AEM system used in the acquisition phase was the five-frequency Aerodat-DSP 99, with sensor towed at 30 m. The coils were configured in three horizontal coplanar pairs (CP1 ~ 900 Hz; CP2 ~ 4500 Hz; CP3 ~ 33,000 Hz) and two vertical coaxial pairs (CX1 ~ 900 Hz; CX2 ~ 4500 Hz). The flight (LV) and control (LC) lines were spaced 100 m and 500 m apart in the E-W (LV) and N-S (LC) directions, respectively. FDEM data processing was performed in

Geosoft | Oasis Montaj 2022.2 software – Seequent. The apparent conductivity images were interpolated and the hanning and directional cosine filters were applied to remove trends and noise. The mid-frequency apparent conductivity image (4,500 Hz) showed a good signal-to-noise ratio and aided in the correct identification of geophysical structures (figure 3).

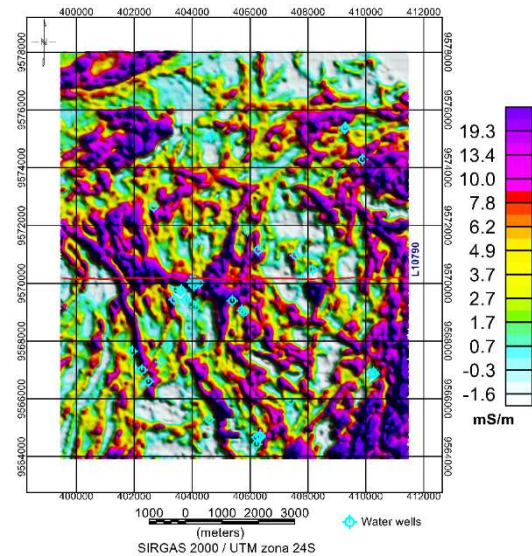


Figure 3- Mid-frequency apparent conductivity image (4,500 Hz, coplanar).

### Results

#### FDEM data inversion (voxel)

The result of the electromagnetic inversion is shown in Figure 4, where we have a three-dimensional image of the conductivity (inversion result;  $S/m$ ) with subreposition of the hydrography (blue); conductive structures (black); geological structures (gray); lithology (red); seismic event epicenter (cube in yellow); and the wells (orange cylinders).

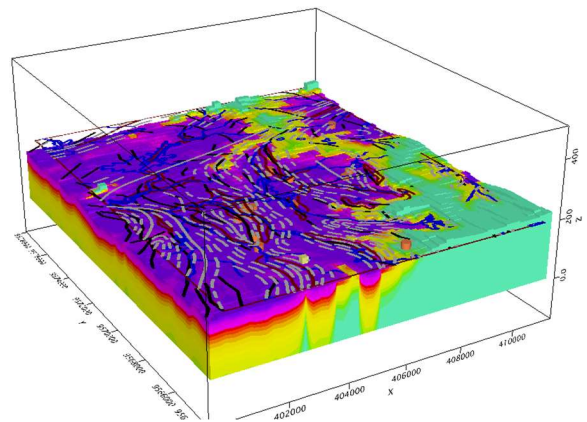
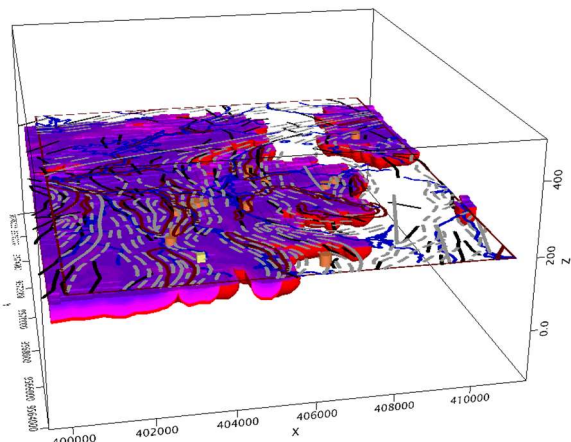
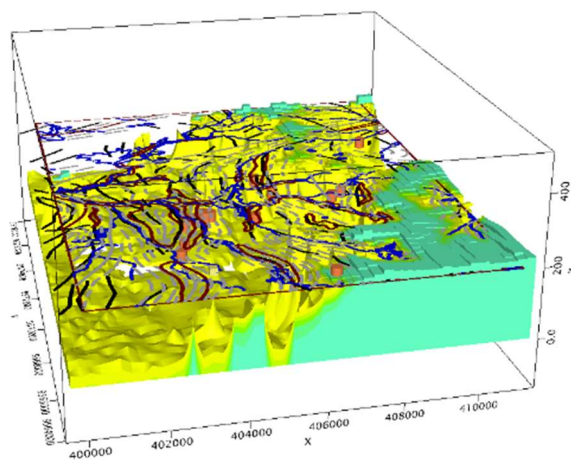


Figure 4- Voxel result of the inversion with the whole area interpolated in S/m.

In the eastern region a conductive layer ( $1.60\text{-}0.003\text{ S/m}$ ) is predominant, varying in elevations from 100 m to 190 m, with an estimated thickness of 50 m (figure 5); under this layer there is a layer of lower conductivity ( $0.0011\text{-}0.003\text{ S/m}$ ) thicker in the eastern region, which reaches 0 m in the western portion. In the western area a resistive layer with conductivity less than  $0.001\text{ S/m}$  and a thickness of 200 m dips to the east (figure 6).



**Figure 5-** Voxel result of the inversion ( $0.003\text{-}1.60\text{ S/m}$ ).



**Figure 6-** Voxel result of the inversion ( $0.0008\text{-}0.0011\text{ S/m}$ ).

As a result of the inversion, Figure 7 shows isosurfaces with conductivity of  $0.00283\text{ S/m}$  (gray);  $0.01\text{ S/m}$  (blue);  $0.0357\text{ S/m}$  (green);  $0.127\text{ S/m}$ ; (yellow) and  $0.451\text{ S/m}$  (red). The deeper layers show lower conductivity and may be associated with the unfractured crystalline basement. Blue and green isosurfaces may be related to rocks altered by fracture networks filled by groundwater. The mid-frequency apparent conductivity image shows high conductivity in the south-central part, which coincides with the red isosurfaces (figure 8) and may be related to the presence of weirs and alluvial deposits. Around the red isosurfaces the gray isosurfaces (figure 9) of lower conductivities ( $0.0028\text{-}0.036\text{ S/m}$ ) prevail.

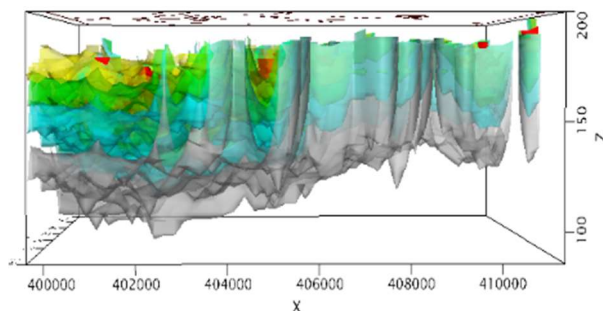


**Figure 7-** Voxel of the isosurfaces with conductivity values from  $0.001\text{ S/m}$  to  $0.451\text{ S/m}$  (vertical exaggeration of 40 in Z).

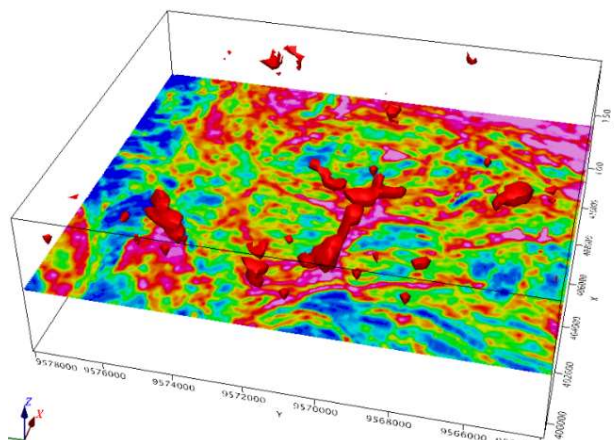


**Figure 8-** Voxel of the red isosurfaces ( $0.451\text{ S/m}$ ) superimposed on the mid-frequency apparent conductivity image.

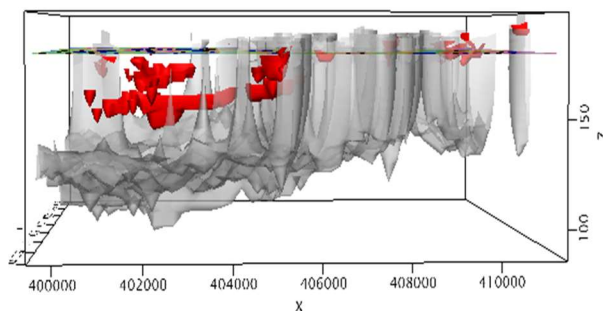


**Figure 9-** Voxel of the red (conductive) and the gray (resistive) isosurfaces.

The section between flight lines 10790 and 10871 contains most of the mapped wells and includes N-S direction amphibolitic bodies, calc-silicate rocks, alluvial deposits, N-S geologic structures, and conductive structures ranging from N-S to NW/SE (figure 10).

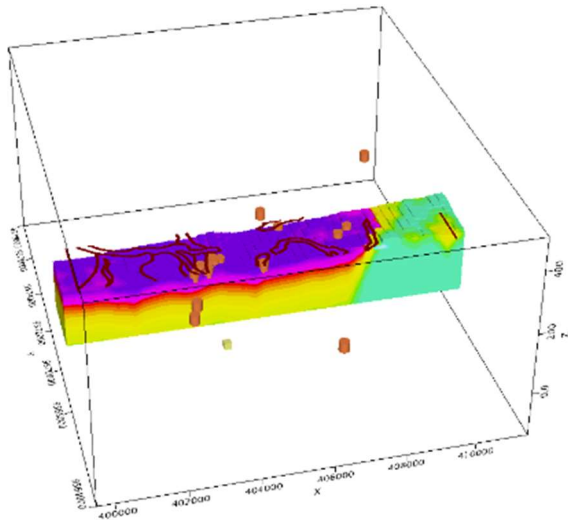


**Figure 10-** Conductivity section between lines 10790 and 10871.

Figure 11 shows an E-W section of the inversion result passing through the epicenter of a seismic event recorded in the area. Note a decrease in conductivity can be seen below this epicenter (yellow cube). Electromagnetic and magnetic lineaments interpreted from conductivity anomalies and the anomalous magnetic field indicate a preferential direction towards N-S. In the northern region, the direction of these lineaments tends towards E-W. These changes are also consistent with changes in the preferred orientations of geological structures. This behavior may be related to the presence of a NE-SW compressional shear zone that possibly exerts structural control in the area. Figure 12 shows a resistive zone below this shear zone.

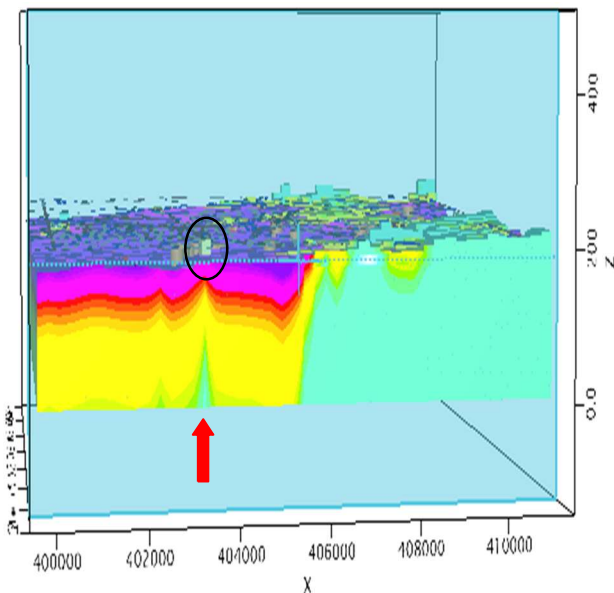


**Figure 11-** Cut at (Y= 9565400) near the epicenter.

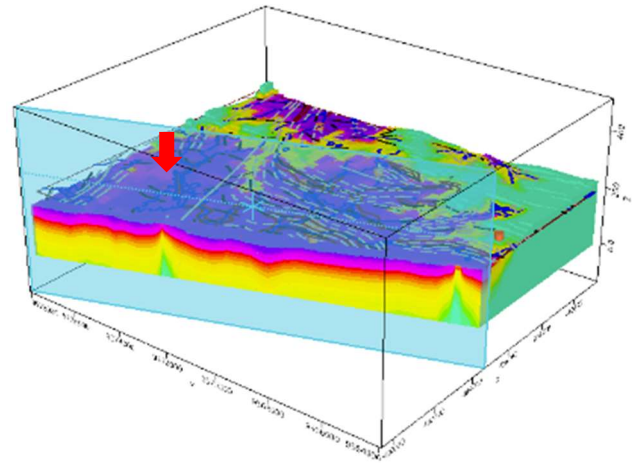


**Figure 12-** resistive area coinciding with the shear zone.

Conductivity-depth

To acquire the CDI's, the Geosoft | Oasis Montaj 2022.2 software calculated the skin depth for each value of conductivity obtained at each frequency (900 Hz, 4,500 Hz and 33,000 Hz) and each coil configuration (coplanar and coaxial).

Noteworthy here is the CDI of line 10790 (figure 13) representative of the wells that had the highest flow rates ( $0.72\text{-}6\text{ m}^3/\text{h}$ ) in the study area.

In general, it is observed that the wells are in areas of intermediate conductivity ( $7.7\text{ mS/m}$ ) reaching more conductive zones ( $18\text{ mS/m}$ ), near magnetic structures with analytical signal amplitude values ranging from  $01\text{ nT/m}$  to  $1.5\text{ nT/m}$  and in topographic low, the latter indicated by the digital elevation model profile.

The wells in this line are concentrated around the São Gabriel weir, which is in a high conductivity zone at coordinates (404000E-406000E). There are more resistive areas at coordinates (400000E-401000E) with conductivity lower than ( $2.0\text{ mS/m}$ ) and magnetic structures with analytical signal amplitude values higher than ( $0.2\text{ nT/m}$ ).

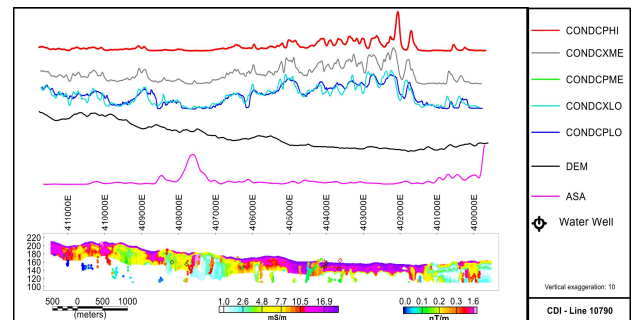


**Figure 13-** CDI (Z component), stacked profiles of the apparent conductivity (coaxial and coplanar), relief (DEM), Analytical Signal Amplitude (ASA), and the Euler solutions.

## Conclusions

In general, the result of the electromagnetic data inversion showed the conductive behavior of the area from the voxel visualization. The consistency of the data inversion with the mid-frequency conductivity image is clearly visible. CDI was efficient in detailing the conductive behavior of the medium in the vicinity of the wells. Anomalous magnetic sources have identified structures and contacts that may be associated with fracture networks in the crystalline environment. This information enriches the knowledge of the region's hydrogeological environment and can guide other projects in the location of groundwater wells, which will reduce the chances of drilling dry wells. The methodology used was important for this work and is a potential tool for mapping water resources of other fractured crystalline environments.

## Acknowledgments

The authors thank the Geological Survey of Brazil-CPRM for making the data available.

## References

- ALMEIDA, F.F.M; HASUI, Y; BRITO NEVES, B.B; FUCK, R.A. 1977. Províncias estruturais brasileiras. In: Simpósio de Geologia do Nordeste, Campina Grande, 363-391.
- ARTHAUD, M. H; VASCONCELOS, A. M; OLIVEIRA, F. V. C. 1998. As Sequências Metassedimentares do Ceará Central. XL Congresso Brasileiro de Geologia. Belo Horizonte. Anais, p.16.
- BEDROSIAN, P. A., SCHAMPER, C., & AUKEN, E. (2016). A comparison of helicopter-borne electromagnetic systems for hydrogeologic studies. *Geophysical Prospecting*, 64(1), 192– 215.
- BEZERRA, F.R.H., et al, 2011. Review of active faults in the Borborema Province, intraplate South America – Integration of Seismological and paleoseismological data. In: *Tectonophysics*, v. 510, n.3, p. 269-290.
- CHONGO, M., CHRISTIANSEN, A. V., TEMBO, A., BANDA, K. E., NYAMBE, I. A., LARSEN, F. 2015. Airborne and ground-based transient electromagnetic mapping of groundwater salinity in the Machile-Zambezi Basin, southwestern Zambia. *Near Surface Geophysics*, Vol. 13(2089), 383–395.
- CORIOLOANO, A. C. F., 2002. Reavaliação de Critérios Estruturais na Hidrogeologia de Terrenos Cristalinos, com Ênfase na Neotectônica e Sensoriamento Remoto. Tese de Doutorado, número 02 / PPGG. Centro de Ciências Exatas e da Terra, Universidade Federal do Rio Grande do Norte.
- ELLIS, R. G., DE WET, B., MACLEOD, I. N., 2012, Inversion of magnetic data for remanent and induced sources. ASEG Extended Abstracts 2012: 22nd Geophysical Conference: pp. 1-4.
- FRASER, D.C., 1978, Resistivity mapping with an airborne multi-coil electromagnetic system: Tulsa, OK, United States, Society of Exploration Geophysicists, *Geophysics* v. 43, p. 144-172.
- KING, J., ESSINK, G.O., KARAOLIS, M., SIEMON, B., BIERKENS, M.F.P. 2018. Quantifying Geophysical Inversion Uncertainty Using Airborne Frequency Domain Electromagnetic Data – Applied at the Province of Zeeland, The Netherlands. *Water Resources Research*, Vol. 54 (10), p. 8420-8441.
- MARQUES, R.M., 1995. Utilização do VLF (Very Low Frequency) na prospecção de água subterrânea em zonas de rochas cristalinas. Dissertação de mestrado, Universidade de São Paulo.
- MCNEILL, J. D. 1991. Use of electromagnetic methods for groundwater studies. In: *Geotechnical and Environmental Geophysics*, Ed. Ward, S. H. Society of Exploration Geophysicists. Series Investigations in Geophysics no. 5 v.1 Review and tutorial. p. 191-218.
- NASCIMENTO DA SILVA, C.C. 2004. Caracterização geológica-geofísica do meio aquífero fissural: uma contribuição aos modelos de fluxo e armazenamento de água subterrânea. Tese de doutorado, Universidade Federal do Rio Grande do Norte.
- PAEPEN, M., HANSSSENS, D., DE SMEDT, P., WALRAEVENS, K., HERMANS, T. 2020. Combining resistivity and frequency domain electromagnetic methods to investigate submarine groundwater discharge in the littoral zone. In: *Hidrology and Earth System Sciences*, Vol. 24 (7), p.3539-3555.
- RICHARTE, D., LUPARI, M., PESCE, A., NACIF, S., & GIMENEZ, M. (2018). 3-D crustal-scale gravity model of the San Rafael Block and Payenia volcanic province in Mendoza, Argentina. *Geoscience Frontiers*, 9(1), 239–248.
- SANTOS DE MENEZES, E.A. 2017. Estudo da Atividade Sísmica em Irauçuba-CE entre setembro de 2015 e março de 2016. Dissertação de mestrado, número 197/PPGG. Centro de Ciências Exatas e da Terra, Universidade Federal do Rio Grande do Norte.
- SATTEL, D. & KGOTLHANG, L. 2004. Groundwater exploration with AEM in the Boteti area, Botswana. *Exploration Geophysics*, 35(2), 147-156.
- SIEMON, B., COSTABEL, S., VOß, W., MEYER, U., DEUS, N., ELBRACHT, J. 2015. Airborne and ground geophysical mapping of coastal clays in eastern Friesland, Germany. *Geophysics*, Vol. 80(3), WB21–WB34.
- SOUZA FILHO, O. A., SILVA, A. M., REMACRE, A. Z., SANCEVERO, S. S., MCCAFFERTY, A. E. & PERROTTA, M. M. 2010. Using helicopter electromagnetic data to predict groundwater quality in fractured crystalline bedrock in a semi-arid region, Northeast Brazil. *Hydrogeology journal*, 18(4), 905-916
- VON HUELSEN, M. G. 2007. Interpretação de dados de Eletromagnetometria aerotransportada (AEM) do sistema Geotem (Domínio do Tempo). Universidade de Brasília - UnB, Distrito Federal, Brasília.: Tese de Doutorado.